Design, Synthesis, and Antifungal Analysis of Pyrazoline Derivatives Against *Candida* Species: A Comprehensive *In Vitro* and *In Silico* Approach

Muhammad Rohim[1], Yuli Haryani[1], Neni Frimayanti[2], Fauzan Zein Muttaqin[3], Hilwan Yuda Teruna[1], and Rudi Hendra[1*]

[1]*Department of Chemistry, Faculty of Mathematics and Natural Sciences, Universitas Riau, Kampus Binawidya, Jl. HR. Soebrantas Km. 12.5, Simpang Baru, Tampan, Pekanbaru, Riau 28293, Indonesia*

[2]*Department of Pharmacy, Sekolah Tinggi Ilmu Farmasi Riau, Jl. Kamboja, Simpang Baru, Tampan, Pekanbaru, Riau 28293, Indonesia*

[3]*Faculty of Pharmacy, Bhakti Kencana University, Jl. Soekarno Hatta No. 754, Bandung 40614, Indonesia*

* ***Corresponding author:***

tel: +62-81365340190
email: rudi.hendra@lecturer.unri.ac.id

Received: March 8, 2025
Accepted: June 10, 2025

DOI: 10.22146/ijc.105255

Abstract: *This study utilized* in vitro *and* in silico *methods to assess the antifungal efficacy of synthesized pyrazoline derivatives (**4a–e**) against* Candida *species. The compounds were produced by a one-pot process and structurally analyzed using spectroscopic methods. The antifungal efficacy was evaluated against* C. albicans, C. glabrata, *and* C. krusei *using minimum inhibitory concentration (MIC) and minimum fungicidal concentration (MFC) assays. Among the derivatives, compound **4e** exhibited potent antifungal action, displaying MIC values similar to ketoconazole. Molecular docking and pharmacophore modeling have shown that **4e** interacts efficiently with critical residues of lanosterol 14α-demethylase (CYP51). The density functional theory (DFT) study indicated advantageous electrical characteristics, while molecular dynamics simulations validated the structural stability of the **4e**–CYP51 complex, evidenced by low RMSD and RMSF values, along with an MM/GBSA binding energy comparable to that of ketoconazole. A robust association between binding energy and MIC substantiates the predictive use of computational data. The results suggest that compound **4e** replicates the binding characteristics of ketoconazole and may be a viable candidate for antifungal medication development. This integrative strategy reinforces the justification for additional optimization and preclinical assessment of pyrazoline-based antifungal drugs aimed at CYP51.*

Keywords: *antifungal activity;* Candida *species; molecular docking; pyrazoline derivatives; structure-activity relationship*

■ INTRODUCTION

Fungal infections cause health problems that affect a population similar to the numbers diagnosed with tuberculosis and malaria together. *Candida* species act as the top fungi, causing infectious diseases, including mucosal diseases, particularly oral thrush, acute vulvovaginal candidiasis, and invasive candidiasis [1]. Fungal infections create major health threats for patients who have weakened immune systems due to cancer treatments, organ transplants, or continuous medication-driven suppression. The expensive battle against *Candida* species persists because these organisms evolved excellent abilities to survive multiple host conditions while successfully evading antifungal medications [2]. While *C. albicans* remains the most prevalent species, increasing reports indicate a rise in the prevalence of non-*C. albicans* species, particularly *C. glabrata* and *C. krusei* [3].

These three species maintain either natural resistance or develop resistance against long-term antifungal medication treatment with azoles, including

fluconazole, that pharmacologists have used since the beginning of the last decade [4]. The scarcity of antifungal drug classes such as azoles, polyenes, echinocandins, and allylamines worsens because these drugs show various toxicities and drug interactions that lead to resistance in different fungal species [5]. The ongoing resistance trend necessitates the immediate development of new antifungal drugs with varying mechanisms of action, according to Vanreppelen et al. [6].

Five-membered heterocyclic compounds classified as pyrazoline derivatives attract interest in medicinal chemistry. They present chemical stability with easy synthesis capabilities and exhibit broad biological activities that extend from antifungal to antibacterial effects and antiviral and anticancer properties [7]. Science shows that these compounds fight fungal infections because they influence essential fungal enzymes, interfere with cellular functions, and block fungal reproduction [8]. The potential of pyrazoline derivatives exists, yet their biological understanding, structure-activity relationships, and mechanisms of action remain unclear to scientific research.

Computational approaches serve as valuable tools for drug discovery and optimization using molecular docking and pharmacophore modeling and density functional theory (DFT) analysis to predict biological activity and study protein-target interactions refined molecular properties [9]. Molecular docking technology mimics target-ligand interactions by forecasting the binding strength as well as the activity mechanism [10]. Pharmacophore models help drug designers identify mandatory structural elements needed for molecular activity through their ability to streamline rational drug development [11]. The electronic properties of potential drug candidates and their stability and reactivity will be evaluated further through DFT calculations to optimize these candidates [12]. The application of computational approaches has not been fully exploited for antifungal pyrazoline research.

Pyrazoline-derived antifungal drug development faces limitations due to insufficient integration of synthetic, computational, and experimental research approaches [13]. The authors propose that modifying the pyrazoline backbone structure will improve fungal enzyme binding and enhance antifungal drug performance. Different pyrazoline derivative compounds demonstrate potential antifungal properties according to computational modeling, which confirms the possibility of beneficial ligand-target binding.

This research uses minimum inhibitory concentration (MIC) and minimum fungicidal concentration (MFC) assessment methods to synthesize pyrazoline compounds through a single-pot procedure before conducting antifungal tests against *Candid*a species. The study performed molecular docking simulations to investigate how ligands bind to target proteins from fungi. The essential features needed for activity determination were identified through pharmacophore modeling methods, which enabled future optimization to be done rationally. The compounds' electronic properties, energy gaps, and molecular stability became clearer through DFT studies, and these findings helped enhance their antifungal properties.

■ EXPERIMENTAL SECTION

Materials

This study used 2-chlorobenzaldehyde, 3-bromobenzaldehyde, 2-methoxybenzaldehyde, 4-chlorobenzaldehyde, and 4-fluorobenzaldehyde to synthesize pyrazoline derivatives, as well as 2-hydroxyacetophenone, 3,4-dimethoxyacetophenone, 4-methoxyacetophenone, and phenylhydrazine from Sigma Aldrich. Recrystallization employed methanol, while thin-layer chromatography (TLC) used silica gel plates from Merck and the corresponding mobile-phase solvents. Analytical characterization included Fourier-transform infrared (FTIR) spectroscopy with potassium bromide, nuclear magnetic resonance (NMR) spectrum analysis with deuterated chloroform and dimethyl sulfoxide-d_6, and ultraviolet-visible (UV-vis) spectroscopic-grade methanol. A high-resolution mass spectra (HRMS) test was performed in this study utilizing appropriate solvents and calibration standards. Sabouraud Dextrose Agar (SDA) and Sabouraud Dextrose Broth (SDB) were used as culture media in

antifungal screening, with resazurin as an indicator and Candida species (*C. albicans* ATCC 10231, *C. glabrata* ATCC 15126, and *C. krusei* ATCC 14243) as test microorganisms. In addition, ketoconazole was used as a positive control in this study.

Instrumentation

All reagents and solvents were purchased from Merck and Sigma Aldrich. Fisher John melting point apparatus (SMP 11-Stuart®) comprised the analytical instruments and equipment utilized in this investigation. A Cole-Parmer® UV lamp was employed to visualize compounds at wavelengths of 254 and 366 nm. The Genesys 10S UV-vis spectrophotometer (v4.002, serial number 2L9N175013) was employed to conduct spectrophotometric analyses. The UPLC Prominence-Shimadzu system, which was equipped with LC Solution software and a UV detector (SPD 20AD), was employed to conduct high-performance liquid chromatography (HPLC) analyses. The samples' infrared spectra were obtained using a Shimadzu IR Prestige-21 spectrophotometer for FTIR spectroscopy. The Water LCT Premier XE mass spectrometer was employed in positive ion mode to conduct mass spectrometric analyses. The Agilent 500 MHz ^{1}H-NMR spectrometer was employed to elucidate the molecular structure.

Procedure

Synthesis pyrazoline derivatives

Aldehyde (1 mmol), ketone (1 mmol), and phenylhydrazine (2 mmol) were reacted in a reactor tube with a 3 M NaOH catalyst (1 mL) using monowave irradiation at 80 °C for 2 h with a stirring speed of 1000 rpm. TLC by using *n*-hexane and ethyl acetate was employed to confirm the reaction, and reverse-phase high-performance liquid chromatography (RP-HPLC; C_{18}, water-acetonitrile over 20 min) was applied to assess the purity of the synthesis results (Fig. 1). All the spectroscopy data can be accessed from https://zenodo.org/records/15508412 and are shown in Fig. S1–S18.

2-(5-(2-Chlorophenyl)-1-phenyl-4,5-dihydro-1*H*-pyrazol-3-yl)phenol (4a). Yellow crystal (MeOH); yield 85.39%; m.p. 99–100 °C UV (MeOH) λ_{max} 306 nm; FTIR (Kbr) ν_{max} 3144, 3063, 2928, 1597, 752 cm^{-1}; ^{1}H-NMR (500 MHz, CDCl3) δ 10.76 (*s*, 1H); 7.48 (*dd*, *J* = 7.9 & 1.3 Hz, 1H); 7.31–7.23 (*m*, 5H); 7.20 (*td*, *J* = 7.5 & 1.3 Hz, 1H); 7.16 (*dd*, *J* = 7.8 & 1.6 Hz, 1H); 7.07 (*dd*, *J* = 8.2 & 1.1 Hz, 1H); 6.94–6.85 (*m*, 4H); 5.63 (*dd*, *J* = 12.4 & 7.0 Hz, 1H); 4.10 (*dd*, *J* = 17.3 & 12.4 Hz, 1H); 3.18 (*dd*, *J* = 17.3 & 7.0 Hz, 1H); HRMS *m/z* 349, 1108 [M+H]$^+$, calcd for $C_{21}H_{17}ClN_2O$, *m/z* 349, 1109.

2-(5-(3-Bromophenyl)-1-phenyl-4,5-dihydro-1*H*-pyrazol-3-yl)phenol (4b). White crystal (MeOH); Yield: 62.21%; m.p. 242–244 °C UV (MeOH) λ_{max} 369 nm; FTIR (KBr) ν_{max} 2998, 2953, 1600,1513, 682 cm^{-1}. ^{1}H-NMR (500 MHz, $CDCl_3$) δ 10.73 (*s*, 1H); 7.53 (*s*, 1H); 7.44 (*dt*, *J* = 7.7 & 1.7 Hz, 1H); 7.31–7.22 (*m*, 5H); 7.13 (*dd*, *J* = 7.7 & 1.6 Hz, 1H); 7.08 (*d*, *J* = 8.2 Hz, 1H); 6.96 (*d*, *J* = 8.1 Hz, 2H); 6.93–6.86 (*m*, 2H); 5.19 (*dd*, *J* = 12.4 & 7.6 Hz, 1H); 3.98 (*dd*, *J* = 17.2 & 12.4 Hz, 1H); 3.25 (*dd*, *J* = 17.2 & 7.6 Hz, 1H); HRMS *m/z* 393,0602 [M+H] calcd for $C_{21}H_{17}BrN_2O$, *m/z* 393, 0603.

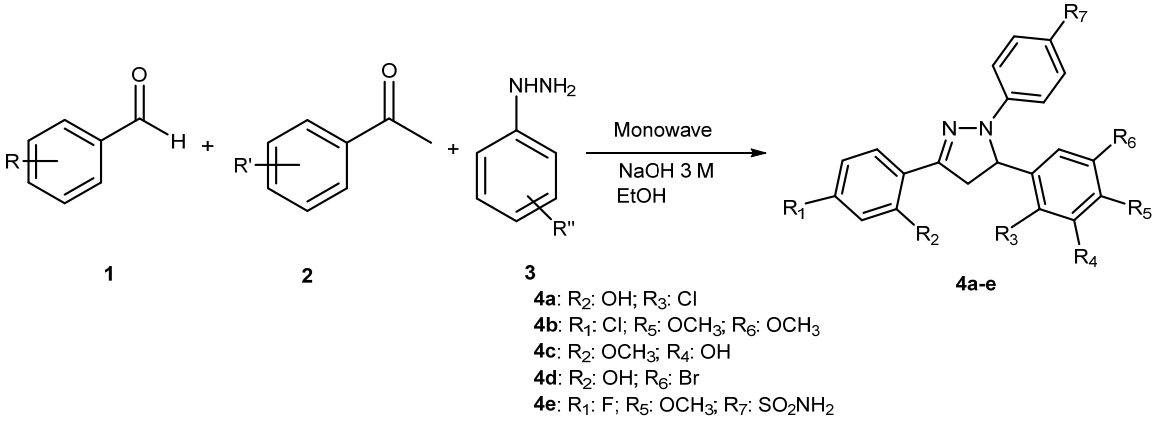

Fig 1. One-pot synthesis of pyrazoline compounds

3-(3-(2-Methoxyphenyl)-1-phenyl-4,5-dihydro-1*H*-pyrazol-5-yl)phenol (4c). Brownish-yellow crystals (MeOH); Yield: 98.83%; m.p. 139–140 °C; UV (MeOH) λ_{max} 356 nm; FTIR (KBr) 3359, 3014, 2947, 1596, 1499, 1381, 1134 cm^{-1}; ^{1}H-NMR (500 MHz, $CDCl_3$) δ 3.30 (*dd*, *J* = 18.0 & 7.6 Hz, 1H); 3.82 (*s*, 3H); 3.93 (*dd*, *J* = 18.0 & 12.3 Hz, 1H); 4.89 (*s*, 1H); 5.14 (*dd*, *J* = 12.3 & 7.6 Hz, 1H); 6.73 (*dd*, *J* = 8.2 & 2.5 Hz, 1H); 6.81–6.76 (*m*, 2H); 6.95–6.89 (*m*, 2H); 7.01 (*t*, *J* = 7.5 Hz, 1H); 7.07 (*d*, *J* = 8.2 Hz, 2H); 7.21 (*dt*, *J* = 17.9 & 7.6 Hz, 3H); 7.32 (*t*, *J* = 7.8 Hz, 1H); 8.01 (*dd*, *J* = 7.7 & 1.8 Hz, 1H); HRMS *m/z* 345, 1603 [M+H], calcd for $C_{22}H_{20}N_2O$, *m/z* 345, 1605.

3-(4-Chlorophenyl)-5-(3,4-dimethoxyphenyl)-1-phenyl-4,5-dihydro-1*H*-pyrazole (4d). White crystal (MeOH); Yield: 75.31%; m.p. 108–109 °C; UV (MeOH) λ_{max} 364 nm; FTIR (KBr) 3008, 2910, 1599, 1521, 754 cm^{-1}; ^{1}H-NMR (500 MHz, $CDCl_3$) δ (ppm): 7.66 (*d*, *J* = 8.6 Hz, 2H); 7.36 (*d*, *J* = 8.6 Hz, 2H); 7.23–7.16 (*m*, 2H); 7.09 (*d*, *J* =7.4 Hz, 2H); 6.89 (*dd*, *J* = 8.2 & 2.0 Hz, 1H); 6.82 (*d*, 1H); 5.22 (*dd*, *J* = 12.3 & 7.7 Hz, 1H); 3.85 (*d*, *J* = 20.3 Hz, 6H); HRMS *m/z* 393, 1370, calcd for $C_{23}H_{21}ClN_2O$, *m/z* 393, 1372.

4-(3-(4-Fluorophenyl)-5-(4-methoxyphenyl)-4,5-dihydro-1*H*-pyrazol-1-yl)benzenesulfonamide (4e). Pale yellow solids (MeOH); Yield: 93.65%; mp 154–156 °C; UV (MeOH) λ_{max} 273 nm; FTIR (KBr) 3254, 3074, 2837, 1592,1502, 1155, 1096 cm^{-1}; ^{1}H-NMR (500 MHz, DMSO) δ 7.86–7.79 (*m*, 2H), 7.58 (*d*, *J* = 8.6 Hz, 2H), 7.26 (*q*, *J* = 8.3 & 7.9 Hz, 3H), 7.10 (*d*, *J* = 8.3 Hz, 1H), 7.03–6.96 (*m*, 4H), 6.84 (*dt*, *J* = 14.6 & 7.2 Hz, 2H), 5.72 (*dd*, *J* = 12.1 & 5.1 Hz, 1H), 3.98–3.88 (*m*, 4H), 3.10 (*dd*, *J* = 17.7 & 5.1 Hz, 1H); HRMS *m/z* 426, 1288, calcd for $C_{22}H_{21}N_3O_3SF$, *m/z* 426, 1279.

In vitro *antifungal activity*

Preparation of media and cultivating fungi. SDA and SDB were employed to cultivate fungal cultures. Cultures of *C. albicans*, *C. glabrata*, and *C. krusei* were cultivated on SDA slant agar utilizing a cross-streaking technique. The cultures were incubated at around 37 °C for 1–2 d to promote regrowth and proliferation.

MIC determination. The assay method was followed by Army et al. [14] and Hendra et al. [15]. Microdilution method in 96-well microplate format was used to determine the MIC. *C. albicans*, *C. glabrata*, and *C. krusei* were cultured in SDB and standardized to an optical density of approximately 0.02 at 530 nm. Varying concentrations were achieved by preparing serial two-fold dilutions of the test samples. As much as 50 µL of growth medium and 10 µL of resazurin indicator were added to each well of microplate and 10 µL of prepared fungal suspension was used to fill each well. Ketoconazole served as positive control and control wells without antifungal agent were utilized as negative controls. The microplate was incubated at 37 °C for 24 h. The MIC was determined by visually comparing and scoring color changes in the wells to that of the negative control wells, an indication of fungal growth.

MFC determination. The assay method was followed by Army et al. [14] and Hendra et al. [15]. The MFC was assessed on SDA plates. Into a sterile petri dish, 25 mL of SDA was poured and allowed to solidify on a sterile plate. Then, 10 µL of each test solution (equal to its MIC) was spread on a solidified SDA's surface. The inoculated plates were incubated at 37 °C for 24 h. Visually, MFC was assessed by observing absence of colonized fungal colonies and the clarity of SDA medium when plates were placed on the day of final reading indicating fungicidal activity.

In silico antifungal activity

Molecular docking. ChemDraw Professional 15.0 served to construct the molecular structures of the studied pyrazoline ligands together with ketoconazole as a positive control. Molecular Operating Environment (MOE) 2022.0902 generated three-dimensional structures from the initial structures using the MMFF94x force field during an energy minimization run with a gradient setting of 0.0001. The 3LD6 protein structure obtained from www.rcsb.org Protein Data Bank served as input for analysis between MOE 2022.0901 and Discovery Studio Visualizer (DSV, Biovia). An optimization of the receptor conformation for interaction was done through energy minimization using CHARMM27 force field, resulting in a root mean square (RMS) gradient of 0.01 kcal/mol. Through the Site Finder function in MOE, the active site identification process for molecular docking began. The

docking system used 50 poses and 10 refinements, and the triangle placement algorithm was used to determine the position, which revealed information about ligand-receptor bonding [15].

Pharmacophore. Pharmacophore Query Editor and Protein-Ligand Interactions Fingerprints are utilized to construct and configure pharmacophores within the MOE 2022.0902 software package. The identification of pharmacophore characteristics commences with the alignment (superposition) of the protein obtained from the RCSB database. The alignment seeks to identify structural similarities among ligands with potential antifungal activity. This study utilized three primary properties for alignment: hydrophobic atoms, hydrogen bond donors, and aromatic rings. Furthermore, all receptors and solvents associated with the preceding protein macromolecule are eliminated, ensuring that only the aligned ligands are displayed in the MOE window [15].

DFT study. DFT calculations were conducted using the Becke three-parameter hybrid functional (B3LYP) in combination with the 6-31G(d,p) basis set and the Lee-Yang-Parr correlation functional, implemented via the Gaussian 09 software platform with GaussView 9 interface. The computational protocol involved initial conformational searches to explore possible molecular conformers, followed by geometry optimization, frequency analysis, and molecular electrostatic potential (MEP) mapping for each structure. Frequency calculations were performed to ensure that each optimized geometry corresponded to a true energy minimum, as indicated by the absence of imaginary frequencies [15].

Subsequently, the optimized neutral molecules were used as the basis for further calculations to determine ionization potential (IP), electron affinity (EA), chemical potential (μ), chemical hardness (η), and electrophilicity index (ω). Single-point energy calculations were carried out on each molecule's optimized neutral, cationic, and anionic forms to obtain their respective total energies. The IP was calculated as the energy difference between the cation and the neutral species, while the EA was determined from the energy difference between the neutral and anionic species. Additionally, the frontier molecular orbital energies (HOMO and LUMO) were extracted from the neutral molecule to compute μ, η, and ω using Eq. (1–3). Consistent computational parameters were maintained throughout to ensure the accuracy and comparability of the calculated molecular descriptors.

$$\mu = \frac{E_{HOMO} - ELUMO}{2} \quad (1)$$

$$\eta = E_{LUMO} - E_{HOMO} \quad (2)$$

$$\omega = \frac{\mu^2}{2\eta} \quad (3)$$

Molecular dynamics (MD) simulation. MD simulations were conducted using the AMBER version 18 software package to predict the stability of ligand-receptor interactions over time and to simulate their behavior under conditions resembling human physiological environments [16]. The simulation protocol included stages of energy minimization, heating up to 310 K, equilibration, and a production run for 100 ns. The evaluated parameters included root mean square deviation (RMSD), root mean square fluctuation (RMSF), and binding free energy (ΔG) calculated using the MM/GBSA method.

Statistical analysis of binding and activity correlation

Minitab® Version 19 was used to conduct Pearson's correlation analysis on the relationship between MIC values and binding free energy (ΔG) of each drug against *Candida* species. A two-tailed test was used, with significance set at p-value < 0.05.

■ RESULTS AND DISCUSSION

Synthesis of Pyrazoline Derivatives

The one-pot reaction method was selected for the synthesis of pyrazoline derivatives due to its superior efficiency in integrating distinct reaction stages into a single procedure [17]. This method eliminates the need for separating and purifying intermediates, thereby substantially reducing the complexity, time, and material consumption often associated with multi-step synthetic procedures. Moreover, this one-pot method enhances total yield by minimizing the loss of intermediates during purifying operations [18-19]. A monowave irradiation at 80 °C with a stirring speed of 1000 rpm is employed to ensure consistent energy

dispersion in the reaction mixture. Moreover, it facilitates rapid reaction kinetics, consistent response repeatability, and scalability [20]. Furthermore, the incorporation of 3 M NaOH as a catalyst provides an alkaline environment essential for facilitating nucleophilic attack and cyclization, which are pivotal stages in the synthesis of the pyrazoline ring [21].

The reaction mechanism in Fig. 2 begins when aldehydes and ketones blend in a phenyl hydrazine-containing medium. Before intramolecular cyclization occurs, the reaction produces hydrazone intermediates. Cyclization happens through a nucleophilic attack on the carbonyl group that appears in the NaOH basic medium [22-23]. Monowave irradiation uses its energy to overcome reaction barriers that enable quick ring formation of pyrazolines. This green reaction, the controlled and efficient one-pot approach, highlights the robustness of pyrazoline synthesis [24].

The synthesized compounds were comprehensively characterized using spectroscopy techniques to confirm their chemical structures. Among these techniques, ^{1}H-NMR spectroscopy provided crucial insights into the integrity of the pyrazoline ring. Doublets of doublet (*dd*) signals observed within the chemical shift range of 5.0–5.6 ppm correspond to the proton attached to the asymmetric carbon adjacent to the nitrogen atom in the pyrazoline ring. Additionally, signals in the δ 3.0–4.2 ppm range, representing diastereotopic protons on the carbon adjacent to the asymmetric center, were also observed [25]. These distinct splitting patterns confirm the successful formation of the pyrazoline framework. Further structural elucidation was supported by FTIR spectroscopy, which exhibited characteristic peaks at approximately 1596–1600 (C=N) and 3144–3359 cm^{-1} (N–H) [26]. HRMS data provided precise molecular mass values, verifying the elemental compositions and confirming the proposed molecular structures.

Antifungal Activity of Pyrazoline Derivatives

In vitro *antifungal activity*

Pyrazoline derivatives (**4a**–**e**) have been evaluated for antifungal activity against three medically relevant *Candida* species, and their MIC and MFC values were used to determine their potency. A well-characterized antifungal agent, ketoconazole, was used as the reference standard for comparative evaluation. The antifungal efficacy of the derivatives was found to be variable, as evidenced in Table 1, in which compound **4e** showed the most promising effect among all the derivatives.

The antifungal activity of the tested derivatives showed that compound **4e** had the highest potency with MIC values of 100, 50, and 50 μM against *C. albicans*, *C. glabrata*, and *C. krusei*, respectively. In addition, MFC values were measured as 200 μM for *C. albicans* and 100 μM for *C. glabrata* and *C. krusei*. Most importantly, the MFC/MIC ratio for all tested strains stayed ≤4, suggesting a fungicidal mode of action [27]. The MIC values of this activity profile were 50 μM, and the MFC values ranged from 50 to 100 μM, similar to ketoconazole.

However, compounds **4b**–**d** were shown to exhibit moderate antifungal activity towards *C. albicans* (MIC 200 μM) and *C. glabrata* and *C. krusei* (MIC 100 μM).

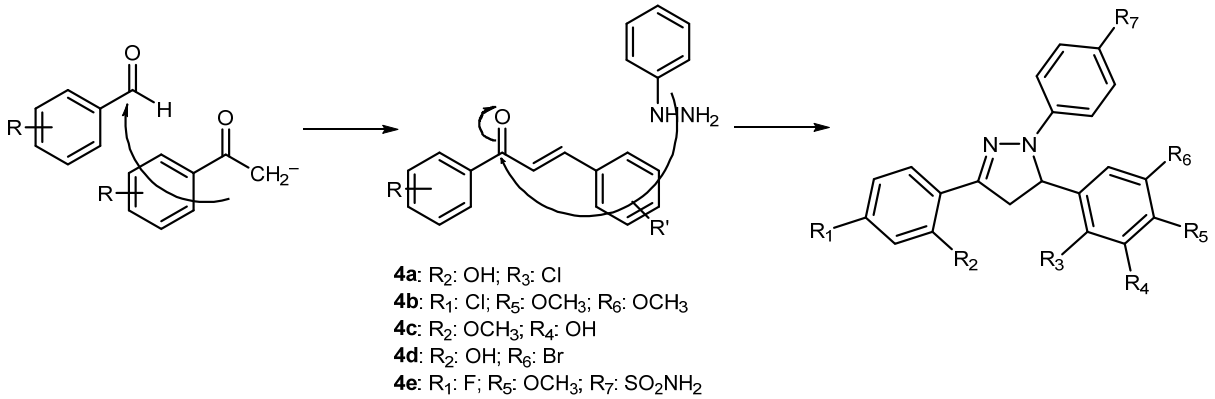

Fig 2. The reaction mechanism for the formation of pyrazoline derivatives

Table 1. Antifungal activity of pyrazoline derivatives (**4a–e**)

Compound	MIC (μM)			MFC (μM)		
	C. albicans	*C. glabrata*	*C. krusei*	*C. albicans*	*C. glabrata*	*C. krusei*
4a	100	100	100	200	>200	>200
4b	200	100	100	>200	>200	>200
4c	200	100	100	>200	>200	>200
4d	200	100	100	200	>200	>200
4e	100	50	50	200	100	100
Ketoconazole	50	50	50	100	50	50

Nevertheless, due to high concentrations of MFC, which exceeded 200 μM, the MFC/MIC ratio was >4, indicating fungistatic effects. Compound **4a** also showed MIC values of 100 μM, but its fungicidal activity was erratic, with MFC values of 200 μM for *C. albicans* and >200 μM for *C. glabrata* and *C. krusei*. The results from these screens suggest that **4e** is the better antifungal and, therefore, is a promising lead compound for antifungal drug discovery.

The structural features of **4e** are likely to contribute to its enhanced activity. The high efficacy of the compound may be due to the substituents that enhance interactions with fungal targets by hydrophobic interactions, hydrogen bonding, or electrostatic forces [28]. Compared with other derivatives, the reduced MIC and MFC values emphasize the significance of precise structural modifications for optimizing antifungal activity.

This corresponds with results from previous studies that demonstrate that para-methoxy and meta-methoxy substitutions increase antifungal potency through enhanced molecular binding to fungal targets [29]. However, this highlights the requirement for structure-activity relationship (SAR) studies in order to develop the rational design of more potent antifungal agents. In general, ketoconazole was more powerful than the pyrazoline derivatives, especially against *C. glabrata* and *C. krusei*. Compound **4e** was similar in activity, and further optimization of this compound as an alternative or adjunct therapy was suggested.

In silico *antifungal activity*

Molecular docking analysis. Molecular docking simulations assessed the binding interactions between antifungal compounds and the essential antifungal enzyme lanosterol 14α-demethylase (CYP51). The research investigated novel inhibitors while examining the existing SAR between tested compounds. Ketoconazole demonstrated the strongest binding free energy of –9.1538 kcal/mol, which indicates a high affinity for CYP51. The binding force between these compounds and CYP51 derives from two hydrogen bonds formed with Phe234 and Ile488, according to Table 2. The enzyme binding also depends on van der Waals forces between Asp231 and hydrophobic bonds that engage Ala311, Leu310, and Met487. Fig. 3 illustrates the critical interactions that show the main residues that drive the antifungal effect of the compound.

Compound **4e** showed the highest binding free energy of –7.5736 kcal/mol among the tested pyrazoline

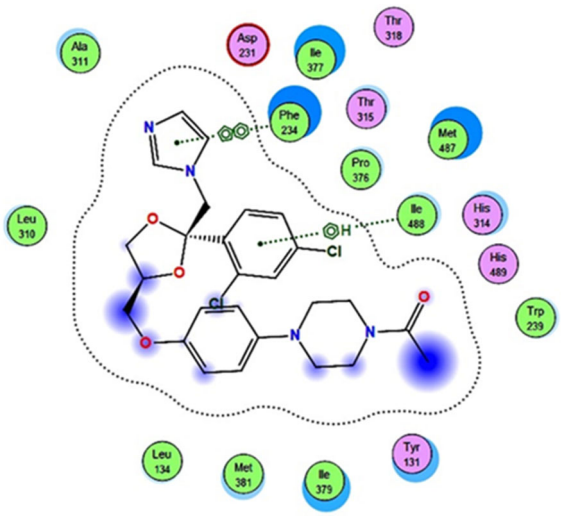

Fig 3. Spatial arrangement of ketoconazole. Green dashed lines indicate hydrogen bonds, π–π interactions, and halogen bonds. Residues are color-coded: green (hydrophobic), purple (polar uncharged), red (acidic), and pink/blue (basic or polar). Blue shading on the ligand highlights hydrophobic interaction regions

Table 2. Molecular docking analysis of pyrazoline derivatives with CYP51

Compound	Binding free energy (kcal/mol)	RMSD	H-bond	Hydrophobic	Van der Waals	Other interactions	Binding factor
Ketoconazole	−9.154	1.836	Phe234, Ile488	-	Asp231	Ala311, Leu310, Ile377, Thr318, Thr315, Pro376, Met487, His314, His489, Trp239, Tyr131, Ile379, Met381, Leu134	17
4a	−6.589	1.541	-	-	Asp231	Ile488, His314, Leu310, Thr315, Phe234, Ala311, Tyr145, Phe139, Tyr131, Thr135, Ile379, Ile377, Met487	11
4b	−7.252	1.282	Cys449	Arg448, Lys156	-	Leu371, Thr315, Ala311, Met380, Tyr131, Ile379, Phe152, Tyr145, His447, Ile377, Ile450, Pro441, Pro376, Phe442	5
4c	−7.014	1.353	Met487, Ile379, Ile377	-	-	His489, Phe234, Met381, Pro376, Met378, Met380, Tyr131, Thr315	8
4d	−7.147	1.585	Met378	-	-	Pro376, Ile379, Ile377, His489, Met487, Thr485, Thr486, Tyr484, Trp239, Met100, Phe105, Phe77, Tyr107, Gly78	6
4e	−7.574	1.539	Arg382, Tyr131	Arg382	Asp231	His489, Met487, Phe234, Ile488, His314, Leu310, Ala311, Met378, Tyr145, Met380, His447, Ile377, Ile379	11

derivatives and was suggested as an antifungal inhibitor. Furthermore, docking analysis showed that **4e** interacted through hydrogen bonds with Arg382 and Tyr161, two key residues within the active site (Table 2). Significant hydrophobic interactions were observed with His489, Met487, and Ile488, and van der Waals interactions with Phe234, Leu310, and Ala311 were appreciated and were consistent with these interactions, as observed in Fig. 4. Spatial placement of **4e** into the active site shows that **4e** has the capacity to fit in the active site and offers the best interactions with the target protein.

Overlay visualization (Fig. 5) of compound **4e** (purple) and ketoconazole (green) produced a comparable binding profile with common critical interaction sites. The structural similarity implies that **4e** acts with a mechanism of action similar to that ketoconazole, and **4e** should be a promising antifungal drug from the structural standpoint. The antifungal properties of pyrazoline derivatives show their highest effectiveness in compound **4e** when considering fluorine along with sulfonamide groups attached to the pyrazoline nucleus structure. The substituents in these compounds improve both the binding properties and biological functioning of CYP51 through essential molecular contacts [30]. The analysis of molecular interactions between pyrazoline derivatives and active site components appears in Table 2 and Fig. 4.

Compound **4e** incorporates fluorine, which strengthens contact with the hydrophobic areas of the active site. The binding pocket of fluorine finds support

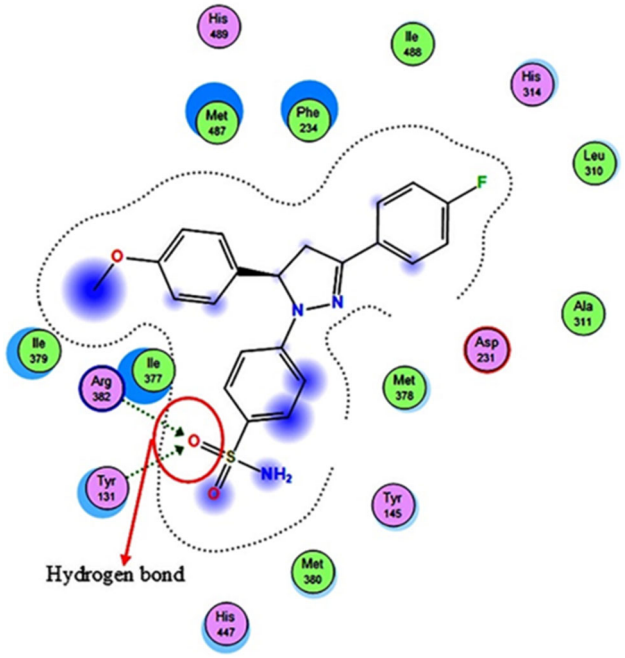

Fig 4. Spatial arrangement of compound **4e.** Green dashed lines indicate hydrogen bonds, π–π interactions, and halogen bonds. Residues are color-coded: green (hydrophobic), purple (polar uncharged), red (acidic), and pink/blue (basic or polar). Blue shading on the ligand highlights hydrophobic interaction regions

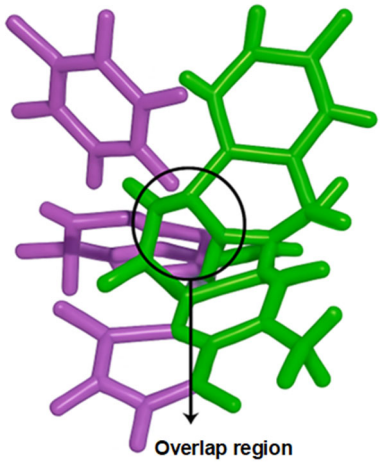

Fig 5. Superimposition of compound **4e** (purple) and ketoconazole (green)

through hydrophobic bonds established between His489, Met487, and Ile488. The electron properties of fluorine in compound **4e** enhance both van der Waals and dipole-dipole interactions, yielding a binding free energy of −7.5736 kcal/mol.

The sulfonamide group significantly boosts hydrogen bond capabilities for antifungal medication. The antifungal activity of the compound increases because the sulfonamide moiety establishes strong hydrogen bonds with Arg382 and Tyr161, which are fundamental active site components that enhance both stability and specificity. Hydrophilic interactions of the sulfonamide group facilitate binding engagement with active site residues, including polar chemical groups [31]. The biological characteristics of compound **4e** with superior MIC and MFC values are attributed to its dual ability to establish hydrogen bonds and enhance solubility through the sulfonamide group (Table 1).

Fig. 4 shows docking visualizations of **4e** achieving the best possible spatial position inside the active site where fluorine and sulfonamide substituents synergize. The antifungal activity of compounds **4a**–**4d** weakens because their substituents have unfavorable positions, leading to higher binding free energy. The docking score optimization in **4e** and its favorable substitution pattern support the improved biological efficiency, as shown in Table 2 and Fig. 4.

A Pearson correlation study was conducted to demonstrate the statistical relationship between the docking free energy of each pyrazoline derivative and the MIC observed during *in vitro* antifungal assays on *Candida* species. The analysis revealed a strong and significant correlation, with a Pearson correlation coefficient (r) of 0.913 and a *p*-value of 0.002. The results indicate that stronger negative binding energy correlates with increased efficacy and a reduced MIC for antifungal compounds.

The robust connection indicates that the binding affinity of the compounds to CYP51 is crucial for their efficacy as antifungals. The findings affirm that CYP51 is a significant target for the pyrazoline derivatives examined in this study. The alignment of predictions with observed outcomes in real organisms illustrates the efficacy of docking simulations as an initial phase in molecular screening for antifungal research. Moreover, this established association validates that the molecular interactions demonstrated by docking, especially those involving compound **4e**, are authentic biological

phenomena associated with the therapy outcomes reported. Consequently, the integration of molecular docking with experimental procedures and statistical correlation analysis results in a dependable approach for the design of antifungal agents targeting CYP51.

Pharmacophore. Pharmacophore analysis represents a fundamental computational method that enables the detection of essential structural features responsible for drug activity, as per Yang et al. [32]. The research used pharmacophore modeling to evaluate the antifungal properties of ketoconazole against the newly synthesized antifungal compound **4e**, which contains a pyrazoline structure. The pharmacophore models show three essential chemical features, which include hydrogen bond acceptors (HBA) together with hydrogen bond donors (HBD) and hydrophobic regions (Hyd) (Fig. 6). The pharmacophoric properties of ketoconazole appear in Fig. 6(a), which shows compound **4e** in Fig. 6(b) to have structural similarity with ketoconazole. Compound **4e** demonstrates potential ketoconazole-mimetic behavior because its spatial distances measure 4.85 and 6.79 Å.

Pharmacophore analysis demonstrates that hydrogen bond formation contributes essentially to the antifungal action of ketoconazole and compound **4e** in their mechanism of action. The active binding site of CYP51 becomes stabilized by two Phe234 and Ile488 hydrogen bonds in ketoconazole. As compound **4e** interacts more strongly with the active site, hydrogen bonds are established with Arg382 and Tyr161. The formation of hydrogen bonds enhances both ligand-protein complex stability and target specificity, decreasing adverse drug effects [33].

When placed into the active site cavities, the hydrophobic pharmacophore model confirmed powerful hydrophobic interactions that enhance the stability of ketoconazole and **4e** binding. The docked position of **4e** achieved a favorable score of −7.5736 kcal/mol through hydrophobic contacts with Ile377 and Arg382 for better binding affinity. Compound **4e** demonstrates how it reproduces ketoconazole's functional interactions in pharmacophore modeling but uses its distinctive structure to enhance selectivity as an antifungal agent, according to Fig. 6.

DFT study. The electronic properties of a compound and its bioactivity, including antifungal potential, are seen as an essential relationship, and computational analysis using DFT is a key tool for understanding this relationship [34]. Molecular stability, electronic distribution, and reactivity are calculated with DFT, and predictions are made on how compounds interact with essential biological targets for fungi, such as enzymes [35]. Table 3 and Fig. 7 provide supporting evidence of the findings from this analysis.

The electronic reactivity of compounds decides the HOMO–LUMO energy gap through critical analysis [36]. The small distance between HOMO and LUMO orbitals indicates higher reactivity along with a better ability to conduct charge transfer processes that enable protein active site binding [37]. The property becomes vital for antifungal activity because ligands need strong

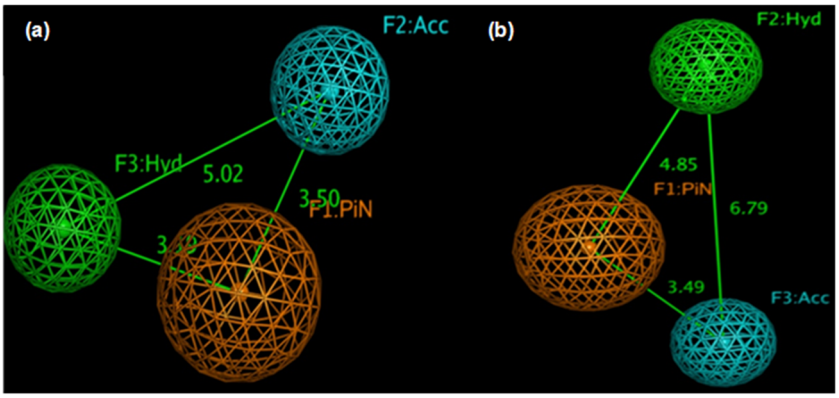

Fig 6. Pharmacophore properties of (a) ketoconazole and (b) compound **4e**

Table 3. Energy, electronic structure, and energy gap of ketoconazole and compound **4e**

Compound	Energy	Electronic structure		Energy gap
		HOMO	LUMO	
Ketoconazole	−2015.50	−0.230	−0.099	0.134
4e	−1560.52	−0.212	−0.080	0.132

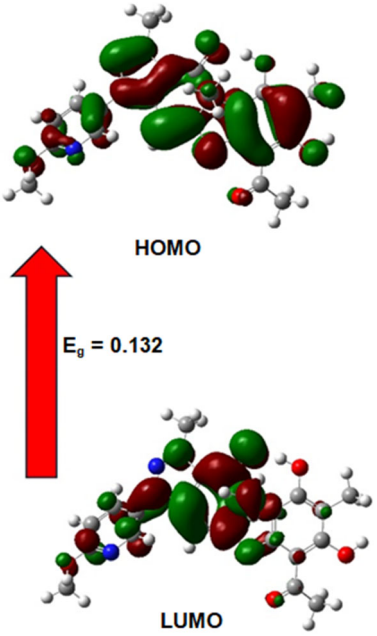

Fig 7. HOMO and LUMO of compound **4e**

binding interactions with CYP51 present in fungi.

Compound **4e** demonstrates electronic reactivity characteristics similar to ketoconazole using HOMO–LUMO gap analysis (Table 3 shows gaps of 0.132 and 0.134 eV). The HOMO and LUMO orbitals of the molecule match the essential CYP51 interaction areas (Fig. 7). The HOMO region facilitates donor interactions, while LUMO orbits near hydrogen bond acceptor sites. Because of its important properties, the docking results indicate that **4e** inhibits CYP51 through electrostatic docking interactions. The total energy calculation determines bioactivity levels and molecular stability aids through its assessment. The total energy value of ketoconazole at −2015.50 kcal/mol exceeds that of **4e** at −1560.52 kcal/mol, which shows that ketoconazole demonstrates better stability. Experimental analysis of **4e** orbital distribution shows enough stability for CYP51 bindings between two molecular systems (Fig. 7).

The MEP map illustrates electron distribution patterns that show both hydrogen bond acceptors as regions with negative electron potential and hydrogen bond donors with positive electron potential [38]. The MEP analysis of compound **4e** demonstrates that electron-dense areas match the positively charged elements of Arg382 inside the CYP51 active site. Compound **4e** uses its hydrophobic characteristics to connect with non-polar residues in the binding pocket to stabilize the formation of ligand-receptor complexes. The pharmacophore model identifies hydrogen bond donors, hydrogen bond acceptors, and hydrophobic regions because they act as essential antifungal activity determinants.

DFT analysis generates compound electronic properties that determine how effectively the compound interacts with target proteins. The dual HOMO donor interactions and LUMO acceptor interactions located within compound **4e** support evidence-based hydrogen bond formation with Arg382 and Tyr161 and thus prevents CYP51 enzyme function. The antifungal effectiveness of compound **4e** receives support from DFT analysis, which also serves as a predictive framework for bioactivity optimization. The antifungal potential can be enhanced by making structural changes that boost hydrogen bond donors/acceptors along with hydrophobicity optimization to lower the HOMO–LUMO gap.

To enhance comprehension of the electronic reactivity and bioactivity potential of compound **4e** relative to ketoconazole, various quantum chemical reactivity descriptors were computed in accordance with Koopmans' theorem. The descriptors encompass IP, EA, η, μ, and ω, as illustrated in Table 4.

These descriptors quantitatively represent the chemical stability and reactivity of the substances. Compound **4e** demonstrates superior chemical hardness (η = 4.55 eV) relative to ketoconazole, signifying enhanced resistance to electronic deformation and potentially increased stability in binding. In the meantime, its reduced electrophilicity index (ω = 0.066) indicates a diminished propensity to take electrons relative to ketoconazole (ω = 0.152), potentially correlating with a

Table 4. Quantum chemical reactivity descriptors of compound **4e** and ketoconazole derived from DFT calculations

Analysis	**4e**	Ketoconazole
IP (kcal/mol)	−1852.723	−1758.907
EA (kcal/mol)	−442.686	−960.738
LUMO (eV)	1.503	0.859
HOMO (eV)	−3.048	−3.041
μ	−0.772	−1.091
η	4.551	3.901
ω	0.066	0.152

distinct reactivity profile towards the fungal CYP51 enzyme.

Notably, compound **4e** has a lower ionization potential, indicating enhanced resistance to electron removal and a reduced electron affinity relative to ketoconazole. This electronic signature demonstrates its distinctive properties as a prospective antifungal agent. When evaluated in conjunction with molecular docking data, which indicated that **4e** exhibited a strong binding affinity (−7.57 kcal/mol) and advantageous hydrogen bonding with critical residues (Arg382, Tyr131), the calculated reactivity descriptors correspond effectively with the documented bioactivity profile. Thus, the incorporation of DFT-derived descriptors with docking analysis improves the molecular comprehension of antifungal activity. These findings confirm that the electrical architecture and reactivity of compound **4e** promote a robust interaction with the CYP51 binding site, underscoring its potential as a lead candidate in antifungal medication development.

MD simulations. MD simulations were performed using the AMBER 18 software suite to evaluate protein-ligand complexes' dynamic stability and interaction behavior across time. The simulations utilized ketoconazole as the conventional antifungal drug and compound **4e** as the principal pyrazoline derivative. A comprehensive 100-ns production run was conducted after suitable system equilibration and minimization phases at physiological conditions (310 K, neutral pH).

The RMSD profiles were used to assess the structural integrity of each protein-ligand complex across time. Fig. 8 illustrates that all three systems—comprising the apo-protein (ligand-free), the protein-ketoconazole complex, and the protein-**4e** complex—demonstrated an initial increase in RMSD over the first 20 ns, indicative of conformational adjustment to the simulation conditions. Subsequently, each system attained a stable fluctuation pattern, signifying equilibrium.

The ketoconazole complex exhibited the most significant structural stability of the systems analyzed, with RMSD values stabilizing between 1.4 and 2.0 Å. The complex with compound **4e** exhibited marginally elevated, yet consistently comparable, RMSD values ranging from 1.6 to 2.2 Å. The apo-protein system demonstrated more significant changes (1.8 to 2.6 Å), indicating that the presence of a ligand—particularly ketoconazole and compound **4e**—improves the structural stability of CYP51. The results indicate that compound **4e** stabilizes the protein structure akin to ketoconazole, enhancing its potential as a functional inhibitor.

The RMSF values elucidate individual amino acid residues' flexibility and dynamic behavior during the MD trajectory. Fig. 9(a) and 9(b) illustrate the RMSF profiles for the ketoconazole and compound **4e** complexes, respectively. Significantly, key residues associated with ligand binding—Tyr131, Tyr145, and Met487—demonstrated low fluctuation values, showing negligible atomic displacement and implying robust contact stability.

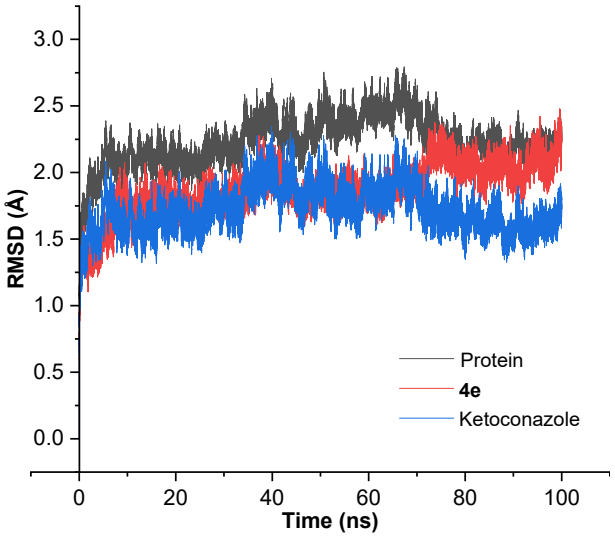

Fig 8. RMSD curve of compound **4e** and ketoconazole

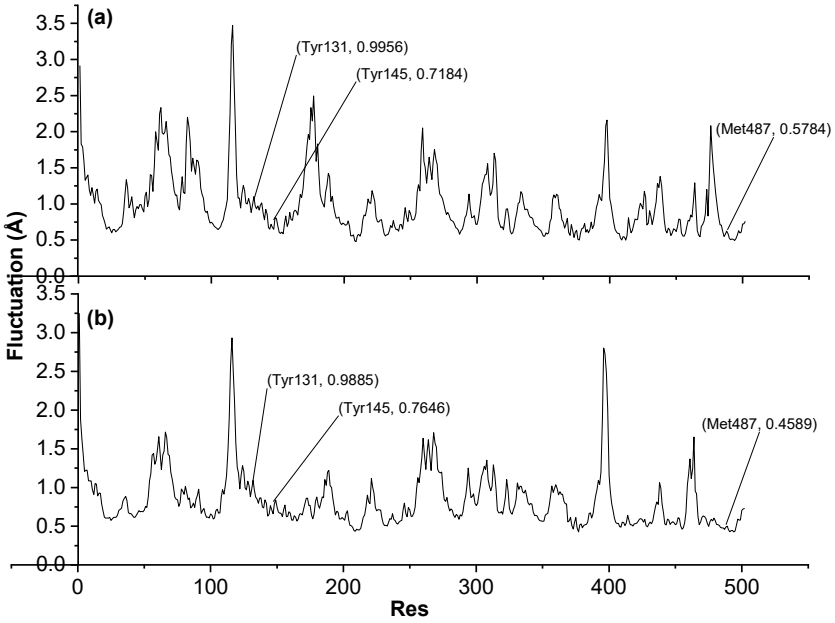

Fig 9. RMSF curve of (a) ketoconazole and (b) compound **4e**

In the ketoconazole complex, the RMSF values for Tyr131, Tyr145, and Met487 were 0.9956, 0.7184, and 0.5784 Å, respectively. The respective residues in the **4e** complex exhibited measurements of 0.9885, 0.7646, and 0.4589 Å. The low RMSF values underscore the capacity of both ligands to maintain the binding pocket, with compound **4e** demonstrating marginally enhanced stabilization of Met487, a residue frequently engaged in hydrophobic and van der Waals interactions [39]. There is a possibility that this characteristic is responsible for the antifungal efficacy of **4e**, which is comparable to that of ketoconazole.

MM/GBSA calculations were performed on equilibrated snapshots from the MD trajectories to quantify the thermodynamic favorability of ligand binding further. The total binding free energy (ΔG_bind) was decomposed into van der Waals (VDWAALS), electrostatic (EEL), polar solvation (EGB), and non-polar solvation (ESURF) contributions (Table 5). The data obtained from the MM/GBSA analysis suggest that both ketoconazole and compound **4e** are capable of forming complexes with CYP51 that are thermodynamically beneficial. The binding energies of these complexes are −18.96 and −17.85 kcal/mol, respectively. Although strong electrostatic interactions (EEL) are the primary force behind the binding of ketoconazole, the compound is also subject to a significant polar desolvation penalty (EGB). Compound **4e**, on the other hand, has more prominent van der Waals contacts, indicating a mainly hydrophobic interaction profile. This profile is less vulnerable to desolvation penalties and may offer improved metabolic and chemical stability *in vivo*.

The fact that the difference in ΔG_total between the two compounds is quite minimal provides further evidence that **4e** is a competitive ligand that possesses promising bioactive potential. This conclusion lends credence to the docking and DFT investigations

Table 5. MM/GBSA binding free energy components for ketoconazole and compound **4e** with CYP51

Energy component (Kkal/mol)	Compounds	
	Ketoconazole	**4e**
VDWAALS	−205.957	−280.145
EEL	−533.143	−11.266
1–4 VDW	0	0
1–4 EEL	0	0
EGB	580.505	15.120
ESURF	−31.043	−38.257
ΔG gas	−73.910	−291.411
ΔG solv	549.463	112.944
ΔG total	−189.637	−178.467

conducted earlier, supplying evidence that **4e** is a potential antifungal lead chemical with CYP51 as its principal molecular target. The MD simulations support the idea that compound **4e**, with its sulfonamide and fluorinated phenyl moieties, forms a stable and energy-efficient contact with the active site of lanosterol 14α-demethylase. The observed stability of functionally important residues, such as Tyr131 and Met487, adds to compound **4e**'s structural compatibility and affinity within the active site. Our findings imply that **4e** not only mimics ketoconazole's binding properties but may also provide extra benefits due to its favorable van der Waals interactions and lower solvation penalties.

The combination of simulation, binding energy breakdown, and residue fluctuation analysis gives a mechanistic explanation for the reported *in vitro* antifungal activity. These findings pave the way for future structural optimization, pharmacokinetic evaluation, and *in vivo* validation of compound **4e** as a potential antifungal treatment candidate.

The *in silico* investigation, which included molecular docking, pharmacophore modeling, DFT, and MD simulations, shows that compound **4e** has strong binding affinity and dynamic stability with the CYP51. The docking study identified essential interactions via hydrogen bonds and hydrophobic contacts, whereas the pharmacophore analysis revealed structural similarities with ketoconazole. DFT-derived electronic descriptors emphasized compound **4e**'s favorable reactivity and MD simulations confirmed its structural stability and long-term association with crucial active site residues. These computational findings reveal a strong chemical basis for compound **4e**'s antifungal action.

These findings are consistent with previous studies reporting that pyrazoline-based compounds possess potent antifungal properties through similar mechanisms of action. This study's antifungal activity observed for compound **4e** aligns well with previous findings on pyrazoline-based scaffolds. For instance, Thach et al. synthesized a series of sulphonamide-substituted pyrazolines. They demonstrated potent activity against *C. albicans*, which was attributed to electron-withdrawing substituents such as 4-Cl or 3-OH groups on the aromatic rings [40]. This supports our observation that the presence of fluorine and sulfonamide groups on compound **4e** may enhance its biological activity through increased lipophilicity and electron density modulation at the binding site.

Similarly, the work by Liang et al. demonstrated the antifungal efficacy of pyrazole amide derivatives against a range of plant pathogenic fungi, where halogen substitution on aromatic rings significantly impacted antifungal performance. Our compound **4e**, containing a fluorinated aryl ring, corroborates this SAR pattern and suggests that halogenation, particularly fluorination, remains a key strategy in designing potent antifungal agents [41]. Desai et al. reported hybrid pyrazole-pyrazoline-pyridine compounds and found several analogs with potent antimicrobial activity, supported by molecular docking analysis that revealed efficient binding at microbial target sites [42]. In our study, docking simulations of compound **4e** also confirmed high binding affinity to the active site of CYP51, with MM/GBSA binding energies comparable to ketoconazole, affirming the consistency of our findings with prior structure-based design studies.

Furthermore, Pathade et al. demonstrated through DFT and docking analyses that fluorinated pyrazolines possess favorable electronic properties and potent bioactivity against *C. albicans* and *Aspergillus niger* [43]. Our DFT calculations also indicated a narrow HOMO–LUMO gap for compound **4e**, indicative of high reactivity and good potential for biological interaction. Together, these comparative analyses validate our experimental results and emphasize the importance of substituent effects, electronic distribution, and computational predictions in the design of antifungal agents based on the pyrazoline scaffold. These findings strengthen the premise that compound **4e** represents a structurally and functionally promising lead compound for further preclinical development.

These *in silico* findings are corroborated by in vitro antifungal activity, with compound **4e** showing MIC and MFC values comparable to ketoconazole against *C. albicans*, *C. glabrata*, and *C. krusei*. Pearson's analysis ($r = 0.913$, $p = 0.002$) demonstrated that the association

between binding free energy and antifungal potency verifies the computational models' prediction accuracy. This comprehensive approach demonstrates compound **4e**'s eligibility as a promising antifungal candidate capable of acting via CYP51 inhibition, justifying its prioritization for future development and preclinical testing.

Nonetheless, the current investigation is restricted by the lack of data on pharmacokinetics, cytotoxicity, and *in vivo* efficacy, all of which are required to assess compound **4e**'s clinical translation potential. Furthermore, computer modeling that considers one fungal target (CYP51) may fail to convey the multifactorial nature of antifungal activity. Future research should examine compound **4e**'s absorption, distribution, metabolism, and excretion (ADME) profile and its selectivity for fungal versus mammalian cytochrome P450 enzymes. *In vivo* efficacy studies in relevant fungal infection models and toxicity testing in mammalian cell lines are required to thoroughly evaluate this compound's therapeutic potential.

■ CONCLUSION

Pyrazoline derivatives **4a**–**4e** were synthesized and assessed for antifungal efficacy. Compound **4e** demonstrated the highest efficacy against the *Candida* species, comparable to ketoconazole. In silico investigations, encompassing molecular docking, DFT, and MD simulations, validated robust binding affinity, electronic stability, and advantageous interaction with CYP51, ascribed to fluorine and sulfonamide substituents. The correlation between computational and in vitro findings substantiates the compound's potential as a primary antifungal agent. Nonetheless, additional *in vivo* validation and cytotoxicity assessments are required. Subsequent efforts will concentrate on biological assessment and structural refinement to improve treatment effectiveness.

■ ACKNOWLEDGMENTS

The authors express gratitude to the Centre of Research and Community Development and the Faculty of Mathematics and Natural Sciences at the University of Riau for the research grant that facilitated this work. The authors wish to pay tribute to Prof. Adel Zamri, whose significant contributions and expert assistance in organic synthesis have greatly enriched our work.

■ CONFLICT OF INTEREST

The authors state that there is no conflict of interest.

■ AUTHOR CONTRIBUTIONS

Muhammad Rohim conducted the experiment, Neni Frimayanti and Fauzan Zein Muttaqin conducted *in silico* studies, Yuli Haryani conducted *in vitro* studies, Rudi Hendra and Hilwan Yuda Teruna wrote and revised the manuscript. All authors agreed to the final version of this manuscript.

■ REFERENCES

[1] Gow, N.A.R., and Netea, M.G., 2016, Medical mycology and fungal immunology: New research perspectives addressing a major world health challenge, *Philos. Trans. R. Soc., B*, 371 (1709), 20150462.

[2] Abdel-Hamid, R.M., El-Mahallawy, H.A., Abdelfattah, N.E., and Wassef, M.A., 2023, The impact of increasing non-*albicans Candida* trends on diagnostics in immunocompromised patients, *Braz. J. Microbiol.*, 54 (4), 2879–2892.

[3] Gómez-Gaviria, M., Ramírez-Sotelo, U., and Mora-Montes, H.M., 2022, Non-*albicans Candida* species: Immune response, evasion mechanisms, and new plant-derived alternative therapies, *J. Fungi*, 9 (1), 11.

[4] Whaley, S.G., Berkow, E.L., Rybak, J.M., Nishimoto, A.T., Barker, K.S., and Rogers, P.D., 2017, Azole antifungal resistance in *Candida albicans* and emerging non-*albicans Candida* species, *Front. Microbiol.*, 7, 2173.

[5] Fuentefria, A.M., Pippi, B., Dalla Lana, D.F., Donato, K.K., and de Andrade, S.F., 2018, Antifungals discovery: An insight into new strategies to combat antifungal resistance, *Lett. Appl. Microbiol.*, 66 (1), 2–13.

[6] Vanreppelen, G., Wuyts, J., Van Dijck, P., and Vandecruys, P., 2023, Sources of antifungal drugs, *J. Fungi*, 9 (2), 171.

[7] Asif, M., Almehmadi, M., Alsaiari, A.A., and Allahyani, M., 2024, Diverse pharmacological potential of different substituted pyrazole derivatives, *Curr. Org. Synth.*, 21 (7), 858–888.

[8] Praveen Kumar, C.H., Katagi, M.S., Samuel, J., and Nandeshwarappa, B.P., 2023, Synthesis, characterization and structural studies of novel pyrazoline derivatives as potential inhibitors of NAD+ synthetase in bacteria and cytochrome P450 51 in fungi, *ChemistrySelect*, 8 (12), e202300427.

[9] Kataria, A., Srivastava, A., Singh, D.D., Haque, S., Han, I., and Yadav, D.K., 2024, Systematic computational strategies for identifying protein targets and lead discovery, *RSC Med. Chem.*, 15 (7), 2254–2269.

[10] Mishra, R., Mishra, P.S., Mazumder, R., Mazumder, A., and Chaudhary, A., 2021, Computational docking technique for drug discovery: A review, *Res. J. Pharm. Technol.*, 14 (10), 5558–5562.

[11] Giordano, D., Biancaniello, C., Argenio, M.A., and Facchiano, A., 2022, Drug design by pharmacophore and virtual screening approach, *Pharmaceuticals*, 15 (5), 646.

[12] Mazurek, A.H., Szeleszczuk, Ł., and Pisklak, D.M., 2020, Periodic DFT calculations—Review of applications in the pharmaceutical sciences, *Pharmaceutics*, 12 (5), 415.

[13] Ebenezer, O., Shapi, M., and Tuszynski, J.A., 2022, A review of the recent development in the synthesis and biological evaluations of pyrazole derivatives, *Biomedicines*, 10 (5), 1124.

[14] Army, M.K., Khodijah, R., Haryani, Y., Teruna, H.Y., and Hendra, R., 2023, Antibacterial *in vitro* screening of *Helminthostachys zeylanica* (L.) Hook. root extracts, *J. Pharm. Pharmacogn. Res.*, 11 (2), 291–296.

[15] Hendra, R., Agustha, A., Frimayanti, N., Abdulah, R., and Teruna, H.Y., 2024, Antifungal potential of secondary metabolites derived from *Arcangelisia flava* (L.) Merr.: An analysis of *in silico* enzymatic inhibition and *in vitro* efficacy against *Candida* species, *Molecules*, 29 (10), 2373.

[16] Case, D.A., Ben-Shalom, I.Y., Brozell, S.R., Cerutti, D.S., Cheatham, III, T.E., Cruzeiro, V.W.D., Darden, T.A., Duke, R.E., Ghoreishi, D., Gilson, M.K., Gohlke, H., Goetz, A.W., Greene, D., Harris, R., Homeyer, N., Huang, Y., Izadi, S., Kovalenko, A., Kurtzman, T., Lee, T.S., LeGrand, S., Li, P., Lin, C., Liu, J., Luchko, T., Luo, R., Mermelstein, D.J., Merz, K.M., Miao, Y., Monard, G., Nguyen, C., Nguyen, H., Omelyan, I., Onufriev, A., Pan, F., Qi, R., Roe, D.R., Roitberg, A., Sagui, C., Schott-Verdugo, S., Shen, J., Simmerling, C.L., Smith, J., Salomon-Ferrer, R., Swails, J., Walker, R.C., Wang, J., Wei, H., Wolf, R.M., Wu, X., Xiao, L., York, D.M., and Kollman, P.A., 2018, *AMBER 2018*, University of California, San Francisco, US.

[17] Hussein, A.J., 2024, Synthesis, antimicrobial and antioxidant activity of some new pyrazolines containing azo linkages, *Curr. Org. Synth.*, 21 (7), 903–916.

[18] Fitri, T.A., Hendra, R., and Zamri, A., 2023, One-pot synthesis and molecular docking study of pyrazoline derivatives as an anticancer agent: Pyrazoline derivatives as an anticancer agent, *Pharm. Educ.*, 23 (2), 260–265.

[19] Farooq, S., and Ngaini, Z., 2020, One-pot and two-pot synthesis of chalcone based mono and *bis*-pyrazolines, *Tetrahedron Lett.*, 61 (4), 151416.

[20] Horikoshi, S., Kamata, M., Mitani, T., and Serpone, N., 2014, Control of microwave-generated hot spots. 6. Generation of hot spots in dispersed catalyst particulates and factors that affect catalyzed organic syntheses in heterogeneous media, *Ind. Eng. Chem. Res.*, 53 (39), 14941–14947.

[21] Pan, D., Mou, C., Zan, N., Lv, Y., Song, B.A., Chi, Y.R., and Jin, Z., 2019, NaOH-promoted chemoselective cascade cyclization of cyclopropyl esters with unsaturated imines: Access to bioactive cyclopenta[c]pyridine derivatives, *Org. Lett.*, 21 (17), 6624–6627.

[22] Jash, M., Das, B., Sen, S., and Chowdhury, C., 2018, Intramolecular cycloaddition approach to fused pyrazoles: Access to 4,5-dihydro-2*H*-pyrazolo[4,3-*c*]quinolines, 2,8-dihydroindeno[2,1-*c*]pyrazoles, and 4,5-dihydro-2*H*-benzo[*e*]indazoles, *Synthesis*, 50 (7), 1511–1520.

[23] Divya, K.V.L., Meena, A., and Suja, T.D., 2016, Unified approach to pyrazole-fused heterocyclic and carbocyclic motifs through one-pot condensation and intramolecular dipolar cycloaddition reaction, *Synthesis*, 48 (23), 4207–4212.

[24] Patel, R.C., Rajani, D.P., Kunjadiya, A., and Patel, M.P., 2024, Microwave accelerated green access to functionalized pyrazolo[5,1-*b*]quinazoline-3-carboxylate scaffold and their pharmacological screening, *J. Mol. Struct.*, 1310, 138295.

[25] Akhtar, W., Marella, A., Alam, M.M., Khan, M.F., Akhtar, M., Anwer, T., Khan, F., Naematullah, M., Azam, F., Rizvi, M.A., and Shaquiquzzaman, M., 2021, Design and synthesis of pyrazole–pyrazoline hybrids as cancer-associated selective COX-2 inhibitors, *Arch. Pharm.*, 354 (1), 2000116.

[26] Praveen Kumar, C.H., Katagi Manjunatha, S., and Nandeshwarappa, B.P., 2023, Synthesis of novel pyrazolic analogues of chalcones as potential antibacterial and antifungal agents, *Curr. Chem. Lett.*, 12 (3), 613–622.

[27] Vieira Melo, A.K., da Nóbrega Alves, D., Queiroga Gomes da Costa, P.C., Pereira Lopes, S., Pergentino de Sousa, D., Queiroga Sarmento Guerra, F., Vieira Sobral, M., Gomes Moura, A.P., Scotti, L., and Dias de Castro, R., 2024, Antifungal activity, mode of action, and cytotoxicity of 4-chlorobenzyl *p*-coumarate: A promising new molecule, *Chem. Biodiversity*, 21 (7), e202400330.

[28] Mishra, S., Kaur, M., Chander, S., Murugesan, S., Nim, L., Arora, D., and Singh, P., 2018, Rational modification of a lead molecule: Improving the antifungal activity of indole – triazole – amino acid conjugates, *Eur. J. Med. Chem.*, 155, 658–669.

[29] Sharma, A., Jain, A.P., and Gangwar, M., 2021, Synthesis, characterization of some new 1,3,5-trisubstituted pyrazole derivatives for their antifungal potential, *J. Pharm. Res. Int.*, 33 (57B), 211–223.

[30] Zarei, A., Ahmadi, Y., and Ramazani, A., 2025, *In silico* investigation on the inhibitory potential of natural polyphenolics against lanosterol 14α-demethylase to discover novel antifungal lead compounds, *J. Mol. Struct.*, 1319, 139499.

[31] Hargrove, T.Y., Friggeri, L., Wawrzak, Z., Qi, A., Hoekstra, W.J., Schotzinger, R.J., York, J.D., Guengerich, F.P., and Lepesheva, G.I., 2017, Structural analyses of *Candida albicans* sterol 14α-demethylase complexed with azole drugs address the molecular basis of azole-mediated inhibition of fungal sterol biosynthesis, *J. Biol. Chem.*, 292 (16), 6728–6743.

[32] Yang, Y.D., He, Y.H., Ma, K.Y., Li, H., Zhang, Z.J., Sun, Y., Wang, Y.L., Hu, G.F., Wang, R.X., and Liu, Y.Q., 2021, Design and discovery of novel antifungal quinoline derivatives with acylhydrazide as a promising pharmacophore, *J. Agric. Food Chem.*, 69 (30), 8347–8357.

[33] Kalinin, S., Kopylov, S., Tuccinardi, T., Sapegin, A., Dar'in, D., Angeli, A., Supuran, C.T., and Krasavin, M., 2017, Lucky switcheroo: Dramatic potency and selectivity improvement of imidazoline inhibitors of human carbonic anhydrase VII, *ACS Med. Chem. Lett.*, 8 (10), 1105–1109.

[34] Yamari, I., Abchir, O., Nour, H., Khedraoui, M., Rossafi, B., Errougui, A., Talbi, M., Samadi, A., Kouali, M.E., and Chtita, S., 2024, Unveiling Moroccan nature's arsenal: A computational molecular docking, density functional theory, and molecular dynamics study of natural compounds against drug-resistant fungal infections, *Pharmaceuticals*, 17 (7), 886.

[35] Alghamdi, S., Abbas, F., Hussein, R., Alhamzani, A., and El-Shamy, N., 2023, Spectroscopic characterization (IR, UV-vis), and HOMO-LUMO, MEP, NLO, NBO analysis and the antifungal activity for 4-bromo-*N*-(2-nitrophenyl) benzamide; Using DFT modeling and *in silico* molecular docking, *J. Mol. Struct.*, 1271, 134001.

[36] Mumit, M.A., Pal, T.K., Alam, M.A., Islam, M.A.A.A.A., Paul, S., and Sheikh, M.C., 2020, DFT studies on vibrational and electronic spectra, HOMO–LUMO, MEP, HOMA, NBO and molecular docking analysis of benzyl-3-*N*-(2,4,5-

trimethoxyphenylmethylene)hydrazinecarbodithioate, *J. Mol. Struct.*, 1220, 128715.

[37] Srivastava, R., 2021, Chemical reactivity theory (CRT) study of small drug-like biologically active molecules, *J. Biomol. Struct. Dyn.*, 39 (3), 943–952.

[38] Suresh, C.H., Remya, G.S., and Anjalikrishna, P.K., 2022, Molecular electrostatic potential analysis: A powerful tool to interpret and predict chemical reactivity, *WIREs Comput. Mol. Sci.*, 12 (5), e1601.

[39] Strushkevich, N., Usanov, S.A., and Park, H.W., 2010, Structural basis of human CYP51 inhibition by antifungal azoles, *J. Mol. Biol.*, 397 (4), 1067–1078.

[40] Thach, T.D., Le, T.T.V., Nguyen, H.T.A., Dang, C.H., Dang, V.S., and Nguyen, T.D., 2020, Synthesis of sulfonamides bearing 1,3,5-triarylpyrazoline and 4-thiazolidinone moieties as novel antimicrobial agents, *J. Serb. Chem. Soc.*, 85 (2), 155–162.

[41] Liang, Z., Rong, Z., Cong, H., Qing-Ying, D., Ming-Zhu, S., Jie, W., Xu-Liang, N., Jin-Zhu, C., Shang-Xing, C., and Da-Yong, P., 2023, Design, synthesis and antifungal activity of novel pyrazole amides derivates, *J. Mol. Struct.*, 1277, 134881.

[42] Desai, N.C., Vaja, D.V., Monapara, J.D., Manga, V., and Vani, T., 2021, Synthesis, biological evaluation, and molecular docking studies of novel pyrazole, pyrazoline-clubbed pyridine as potential antimicrobial agents, *J. Heterocycl. Chem.*, 58 (3), 737–750.

[43] Pathade, S.S., Adole, V.A., and Jagdale, B.S., 2021, PEG-400 mediated synthesis, computational, antibacterial and antifungal studies of fluorinated pyrazolines, *Curr. Res. Green Sustainable Chem.*, 4, 100172.